This article appeared in *Applied Physics Letters 112, 251906 (2018);* and may be found at: https://doi.org/10.1063/1.5040486

Acoustic emission avalanches during compression of granular manganites

Daniel Soto-Parra, Eduard Vives, M. E. Botello-Zubiate, J. A. Matutes-Aquino, and Antoni Planes

Citation: Appl. Phys. Lett. **112**, 251906 (2018); doi: 10.1063/1.5040486
View online: https://doi.org/10.1063/1.5040486
View Table of Contents: http://aip.scitation.org/toc/apl/112/25
Published by the American Institute of Physics

Acoustic emission avalanches during compression of granular manganites

Daniel Soto-Parra,[1,2] Eduard Vives,[1] M. E. Botello-Zubiate,[3] J. A. Matutes-Aquino,[3] and Antoni Planes[1]

[1]*Departament de Física de la Matèria Condensada, Facultat de Física, Universitat de Barcelona, Diagonal, 647, E-08028 Barcelona, Catalonia, Spain*
[2]*Instituto Potosino de Investigación Científica y Tecnológica A.C., Camino a la Presa San José 2055, Col. Lomas 4a, CP 78216 San Luís Potosí, S.L.P., Mexico*
[3]*Centro de Investigaciones en Materiales Avanzados, S. C. Miguel de Cervantes 120, Complejo Industrial Chihuahua, 31109 Chihuahua, Mexico*

(Received 17 May 2018; accepted 5 June 2018; published online 20 June 2018)

We have studied acoustic emission (AE) during compression of $La_{0.8}Ca_{0.28}Sr_{0.08}MnO_{2.7}$ manganites with different microstructures obtained by selected synthesis techniques. In ceramic samples with large grains obtained by a solid-state method, avalanche criticality is confirmed when grain fracture is the AE dominant mechanism. In samples synthesized by means of micro-wave and sol-gel techniques, grains are much smaller and the AE is mainly originated from friction effects associated with relative displacement of grains during deformation. In this case, significant deviations from avalanche criticality have been detected. *Published by AIP Publishing.*
https://doi.org/10.1063/1.5040486

LaCaSrMnO manganites show attractive functional properties associated with a paramagnetic to ferromagnetic transition.[1,2] In the transition region, these materials exhibit rather good magnetocaloric properties, which makes them potentially interesting for refrigeration applications. However, their magnetic properties are affected by the microstructure, which in turn is strongly dependent on the synthesis method. Good properties have been reported in ceramic systems obtained by high temperature sintering of powders. These samples are usually subjected to high temperature annealing to reduce porosity. The consequence is grain growth, which results in very brittle samples. This is detrimental for magnetocaloric applications since crackling during cooling might occur due to anisotropic thermal expansion.[3]

This paper deals with the study of the mechanical behavior of $La_{0.8}Ca_{0.28}Sr_{0.08}MnO_{2.7}$ manganites obtained from selected synthesis methods, which lead to microstructures with different grain sizes and porosities. Mechanical behavior has been studied using the acoustic emission (AE) technique, which enables to follow the progression of failure of the material subjected to an applied stress. This is an interesting technique that provides relevant information about the collective mechanical response of the material during the process. In some cases, it has been reported that AE event features such as signal amplitude, energy, or duration are, to a very good approximation, power law distributed. This behavior defines a class of non-equilibrium criticality usually denoted as avalanche criticality or crackling noise. It is associated with an intermittent sequence of avalanches, which occur in the absence of characteristic scales.[4] It has been reported for many physical processes ranging from externally driven solids,[5–9] to Earth seismicity[10] and stellar evolution.[11]

Recently, this AE statistical method has been used to study failure in synthetic glasses,[12] natural minerals,[13–15] martensitic alloys,[16] wood,[17] bones,[18] among other materials. Avalanche criticality has been confirmed in the case of porous Vycor where the power law behavior has been found in more than nine decades characterised by an energy exponent close to 1.4.[19] However, in general, the power law is much less well defined and the exponent takes values within a relatively broad range from 1.4 to 2. At present, it is no yet clear to which extent these values might be influenced by the microstructure, the porosity, or by a combination of critical and non-critical mechanisms that are operative during the process. The aim of the present paper is to analyse the influence of the microstructure on the avalanche behavior during uniaxial compression of $La_{0.8}Ca_{0.28}Sr_{0.08}MnO_{2.7}$ manganites obtained from micro-wave (MW), sol-gel (SG) and solid-state (SS) synthesis methods.

Samples were prepared starting from a mixture of stoichiometric quantities of lanthanum nitrate of 99.999% purity, calcium nitrate of 99.0% purity, strontium nitrate of 99.0% purity, and manganese nitrate of 97.0% purity, which were dissolved in distilled water and subjected to magnetic stirring during 15 min. Then, citric acid and ethylene glycol were added while keeping stirring for 30 min more.

For hydrothermal synthesis assisted by MW, the solution was transferred to a vial of an Anton Paar Multiwave PRO MW system and sintered in a temperature controlled reaction mode at 250 °C during 60 min. Subsequently, the obtained product was heated up to 110 °C at a rate of 2 °C/min (to eliminate liquid waste), kept at this temperature during 15 min and then heated up to 800 °C at a rate of 30 °C/min and annealed at this temperature during 3 h. Finally, the obtained powders were milled, pressed, and sintered during 3 h at 900 °C, 3 h at 1000 °C, 3 h at 1100 °C, and 3 h at 1200 °C. These samples will be denoted as MW samples.

For Pechini SG chemical synthesis, the solution was maintained at 75 °C until the formation of a gel. The gel was then calcined at a heating rate of 10 °C/min up to 250 °C and annealed during 14 h. Then, thermal treatments at 550 °C during 3 h and 1000 °C during 10 h were carried out. The obtained powder was pressed and sintered at 1200 °C during 6 h. These samples will be denoted as SG samples.

For the SS reaction method, nominal compositions were prepared from high oxides and carbonates of La_2O_3 (99.99%), Mn_2O_3 (99%), $SrCO_3$ (99.9%), and $CaCO_3$ (99.99%), which were mixed in an agate mortar and calcined in a two-stage thermal process: 15 h at 750 °C and 18 h at 950 °C, respectively, with intermediate grindings in a planetary micromill Pulveriste 7 (Fritsh GmbH) between each heat treatment. Finally, the samples were pressed and sintered at 1300 °C for 24 h. These samples will be denoted as SS samples.

SEM images of the microstructure of the samples are shown in Fig. 1. In MW samples, irregular and faceted particles are observed with an average size of 0.4 μm. For SG samples, a granular morphology is found with an average particle size of 1.5 μm. For SS samples, a granular morphology bounded by grain boundaries is observed, with average particles size larger than 3 μm. Porosity decreases as the average grain size increases so that the MW sample appears much more porous than the other two. In all cases, the crystalline structure is the same as confirmed from the x-ray diffraction patterns shown in Fig. 1(d).

Compression experiments were carried out using a mechanical test machine ZMART.PRO (Zwick/Roell). Cylindrical samples, with cross-section $\Phi \simeq 11.3\,\text{mm}^2$, height, $h \simeq 4.3$ mm and mass, $m \simeq 0.16$ g (SG), $\Phi \simeq 6.75\,\text{mm}^2$, $h = 2.5$ mm, $m \simeq 0.09$ g (MW) and $\Phi \simeq 41\,\text{mm}^2$, $h \simeq 3.5$, $m \simeq 0.4$ (SS) were placed between two parallel plates. Compression was applied in the axial direction of the cylindrical samples with no lateral confinement at a constant and low displacement rate of 0.1 mm/min. The force/stress was measured using a load cell, in the range up to a maximum nominal force of 5 kN (with uncertainities $\sim \pm 1$ N).

AE signals were detected using piezoelectric transducers embedded in both plates. The electric output signals were pre-amplified (60 dB), band filtered (between 20 kHz and 2 MHz), and analysed by means of a PCI-2 system from Euro Physical Acoustics (Mistras Group) working at 40 MSPS. We have assumed that an AE event starts at the time t_i at which the pre-amplified electric signal $V(t)$ crosses a fixed threshold of 22 dB, and finishes at time $t_i + \Delta_i$, when, after this time, the signal remains below threshold during a preset time (200 μs). The energy E_i of each signal is obtained from the integration of $V^2(t)$ in the time interval Δ_i divided by a reference resistance of 10 kΩ.

Figure 1(e) shows stress-strain curves. The strain has been estimated as the sample shrinkage, Δh, divided by its initial height h. A significant yield stress is observed in MW and SG samples followed by a stress softening of more than 50%. In contrast, the strain dependence of the stress in the SS sample is much smoother showing a plateau at a rather low stress value and a further tendency to monotonously increase. This different behavior might be related to the different grain size and porosity of the samples. In all cases, a noteworthy increase in stress occurs at the late stages of the process. In this late regime, samples are already fragmented into small grains that remain in the compression plates. The increase in stress is associated with a hardening effect, which might be a consequence of the fracture of these grains.

AE during compression has been detected in all the studied samples. The stress and AE activity (given per unit mass to take into account the different sizes of the studied samples) are depicted as a function of time in Fig. 2. In all samples, a highly non-stationary time evolution of the AE

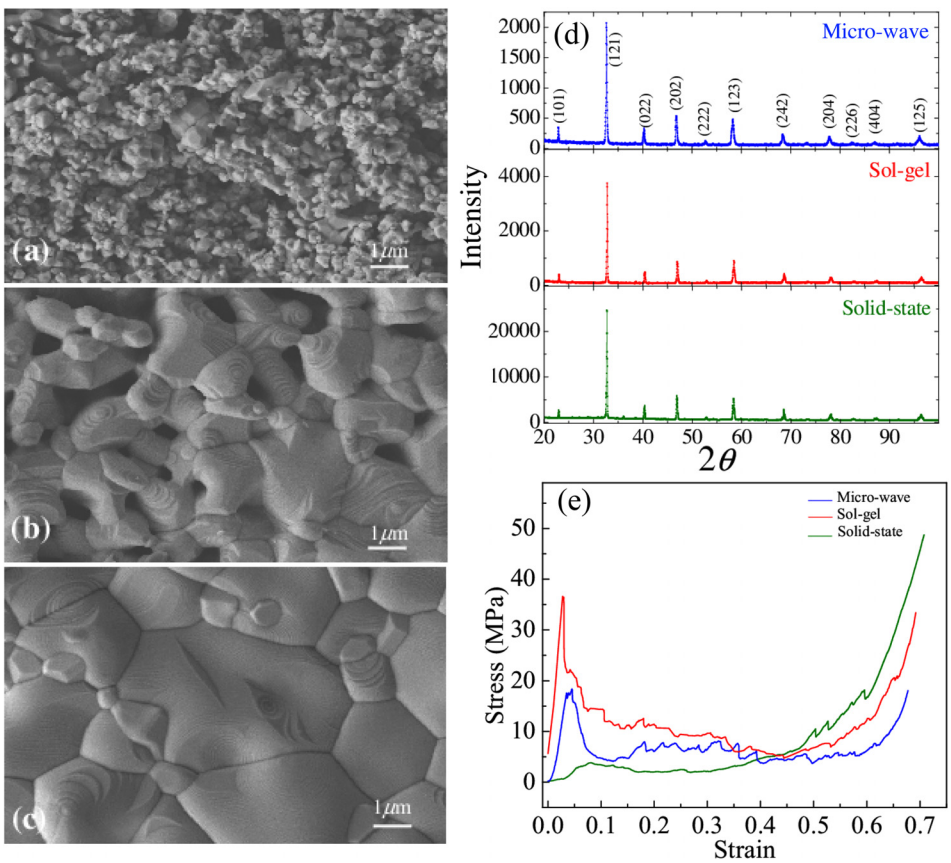

FIG. 1. SEM image of the microstructure of the samples obtained by (a) MW, (b) SG, and (c) SS techniques. The average grain sizes are 0.4 μm, 1.5 μm, and 3 μm, respectively. (d) X-ray patterns and (e) stress-strain curves of the three samples.

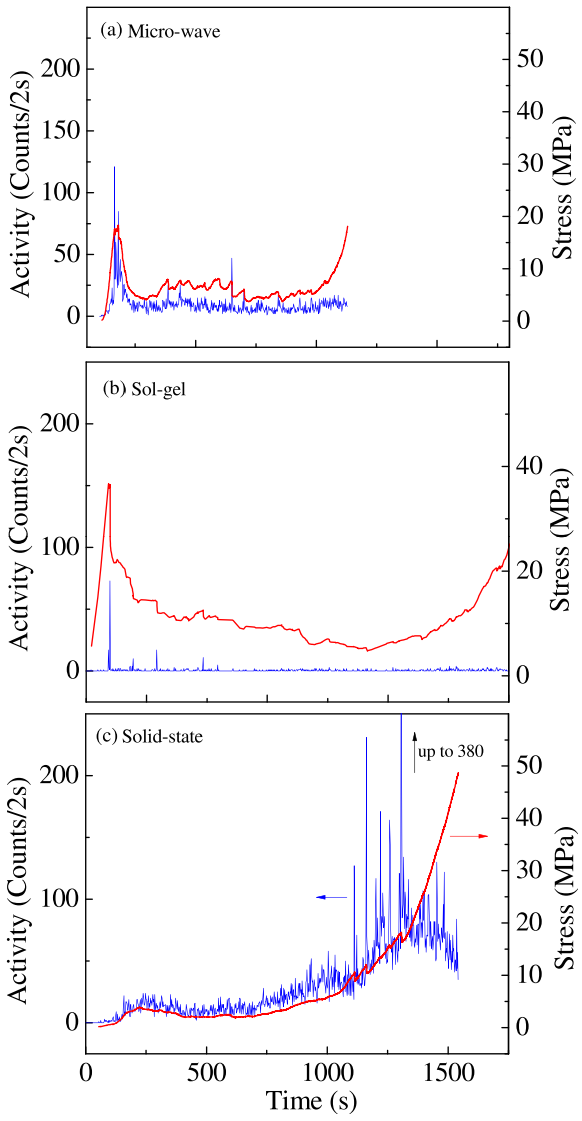

FIG. 2. AE activity (number of hits recorded in time units of 2 s) and stress as a function of time corresponding to (a) MW, (b) SG, and (c) SS samples. Note that for all samples, large AE activity occurs, which is associated with big stress drops.

activity occurs with large peaks well correlated with significant stress relaxation events. For MW and SG samples, most of the AE activity is associated with large stress drops that occur close to the yield stress. Instead, for the SS sample the region of larger AE activity is associated with the stress drops that happens at the late stage hardening region and are probably associated with grain cracking. This different behavior is indeed a consequence of grain characteristics obtained by synthesis of the samples. In general, it is expected that during compression of granular materials two main mechanisms are operative giving rise to deformation and finally to failure: grain breaking and relative grain displacement with associated friction. In all our samples, the AE during early stages is originated from dominant friction effects.

The distribution of the energies of AE events over the full compression process is shown in Fig. 3 in a log-log representation. A first glance suggests an effective linear behavior of the probability distribution over at least three decades, $p(E) \sim E^{-\varepsilon}$, in all the studied samples. To corroborate this behavior, a numerical analysis based on the maximum

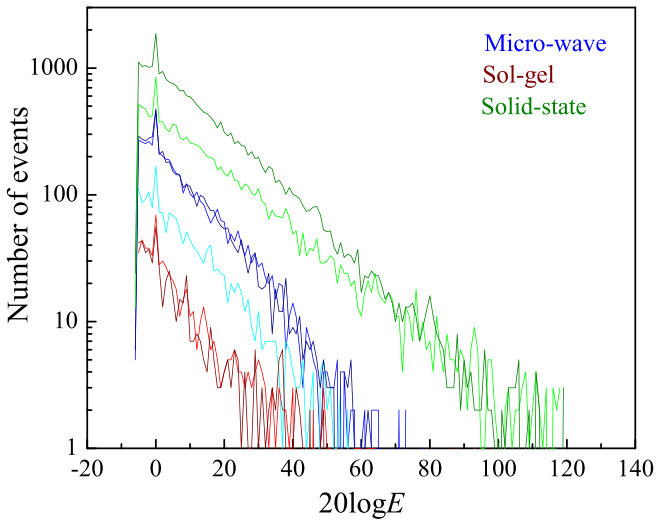

FIG. 3. Energy distributions corresponding to the three studied samples. From each kind of sample, results corresponding to two experiments are depicted.

likelihood method has been performed. This consists of studying the behavior of the exponent ε fitted using the maximum likelihood method as a function of a varying lower cutoff E_{min}.[21] If the process is scale-free (power-law) within a certain range, a plateau of constant exponent will be obtained in the likelihood plot. Deviations from such a plateau can be interpreted in terms of mixing of different mechanisms operating simultaneously during the process or due to the existence of exponential damping effects associated with some characteristic scale.[20]

In our case, a plateau is only well defined over more than four decades in the case of the SS samples. An exponent $\varepsilon = 1.45 \pm 0.05$ is obtained. However, for MW and SG samples, the likelihood plots indicate clear deviations from power law behavior. Actually, in the expected plateau region (cutoff energy in the range between 1 and 100 aJ), the likelihood function shows a significant positive slope in the case of the MW sample, while it shows a kind of parabolic shape in the case of the SG samples. From the analysis reported in Ref. 20, these results suggest that for the MW samples the process is affected by a characteristic scale, while for SG samples, in addition to this effect, the process might be controlled by two mechanisms. In any case, since the obtained behavior could be strongly influenced by late stage effects, we have reanalysed the distribution suppressing the signals detected during this regime. This is shown in Fig. 4 where only signals detected for times lower than 750 s (see Fig. 2) have been considered. No plateau occurs in any of the studied samples. Positive slope is obtained for both MW and SS samples, while a less significant parabolic shape is still obtained in the case of the SG sample.

A complementary analysis can be carried out from the study of duration, D, vs. energy, E, density maps. Maps corresponding to the whole process are shown in Fig. 5 (left column), on a log-log scale. The isolines indicate regions with the same number of counts. An approximate statistical relation $D \sim E^{\nu}$ ($\nu \simeq 0.4$) is obtained for all samples. For the SS sample, the map suggests that two families of signals can be distinguished. The first is constituted of signals with low

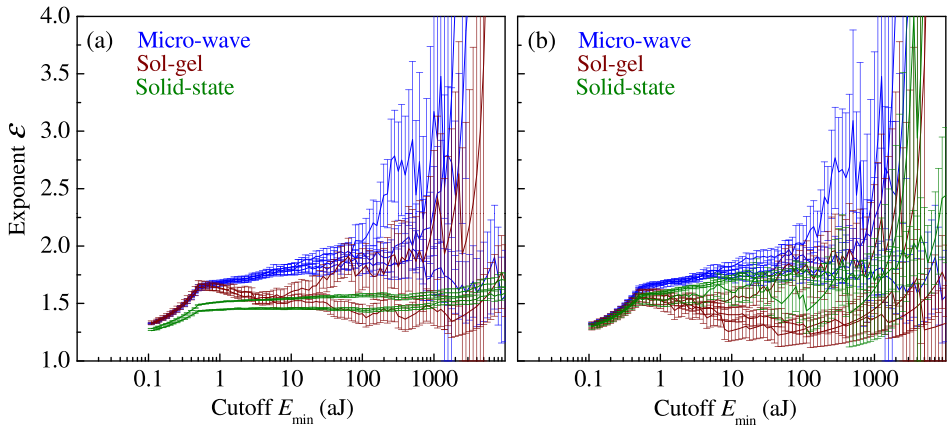

FIG. 4. Likelihood plots corresponding to energy distributions shown in Fig. 3. (a) All recorded data. (b) Only data recorded for $t < 750$ s. The same color code is used.

energies and durations, which show a tendency to deviate from the power law behavior for energies and durations larger than ∼40 dB and ∼60 dB, respectively. The second branch corresponds to higher energy and duration signals. This branch also shows power law statistical behavior. For MW and SG samples the two branches are much less well defined, particularly in the case of the SG sample. This is due to the small number of detected signals.

To establish the influence of AE signals arising from late stages crackling effects, in Fig. 5 (right column), we have replotted the same maps with only the signals recorded before the first 750 s. For the SS sample, the present map does not now contain the second branch corresponding to large energies and durations. This confirms that this branch is constituted of the signals detected in the late compression stages, which are originated from crackling of grains. This effect is much less significant in MW and SG samples, for which the present maps are much more similar to those obtained with the whole set of data. These results confirm the conclusions of the previous analysis based on the likelihood plots.

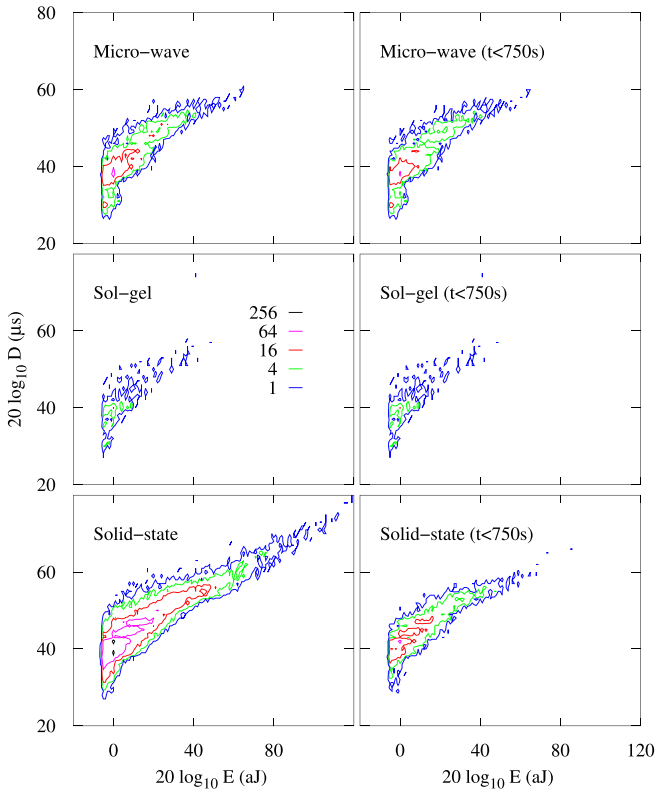

FIG. 5. Energy-duration map. Left: with all data. Right: only data recorded up to $t \leq 750$ s. Contour lines indicate bins with the same number of events. The corresponding numbers are given in the color code.

In conclusion, we have shown that the behavior of the AE detected during the compression of $La_{0.8}Ca_{0.28}Sr_{0.08}MnO_{2.7}$ manganites shows some dependence on the synthesis method, which has a strong influence on the sample grain size and porosity. The statistical analysis of the AE detected during compression indicates that the first stage of deformation is in all cases controlled by the relative displacement of grains. The distribution of the energies of AE signals reveals significant deviations from power law behavior, which reflect that the process does not display avalanche criticality. This behavior is favored by larger porosity as occurs in the MW sample. However, when the AE is dominated by the grain fracture in the hardening region, as in SS samples, avalanche criticality occurs to a very good approximation. The critical exponent, $\varepsilon \simeq 1.45$, is in good agreement with the universal exponent reported for porous Vycor glass, which is a prototypical material displaying crackling criticality during compression.

This research was supported by the Spanish Ministry of Science (Project No. MAT2016-75823-R), CONACYT, Mexico (Project No. IFC 2015-1/635), and the U.S. ARMY Grant Award No. W911NF-16-1-0046.

[1]A. R. Dinesen, S. Linderoth, and S. Mørup, J. Phys. Condens. Matter **17**, 6257–6269 (2005).
[2]N. Pryds, F. Clemens, M. Menon, P. H. Nielsen, K. Brodersen, R. Bjørk, C. R. H. Bahl, K. Engelbrecht, K. K. Nielsen, and A. Smith, J. Am. Ceram. Soc. **94**, 2549–25555 (2011).
[3]K. Zmorayová, V. Antal, J. Kováč, P. Diko, and J. G. Noudem, Acta Phys. Pol. **131**, 804–806 (2017).
[4]J. P. Sethna, K. A. Dahmen, and C. R. Myers, Nature **410**, 242 (2001).
[5]E. Vives, J. Ortín, L. Manosa, I. Ràfols, R. Pérez-Magrané, and A. Planes, Phys. Rev. Lett. **72**, 1694 (1994).
[6]E. Faran, E. K. H. Salje, and D. Shilo, Appl. Phys. Lett. **107**, 071902 (2015).
[7]P. J. Cote and L. V. Meisel, Phys. Rev. Lett. **67**, 1334 (1991).
[8]G. Durin and S. Zapperi, in *The Science of Hysteresis*, edited by G. Bertotti and I. Mayergoyz (Academic Press, San Diego 2006), Vol. II, pp. 181–267.
[9]F. Csikor, C. Motz, D. Weygand, M. Zaiser, and S. Zapperi, Science **318**, 251 (2007).
[10]J. T. Uhl, S. Pathak, D. Schorlemmer, X. Liu, R. Swindeman, B. A. W. Brinkman, M. LeBlanc, G. Tsekenis, N. Friedman, R. Behringer *et al.*, Sci. Rep. **5**, 16493 (2015).
[11]M. A. Sheikh, R. L. Weaver, and K. A. Dahmen, Phys. Rev. Lett. **117**, 261101 (2016).

[12]J. Baró, A. Corral, X. Illa, A. Planes, E. K. H. Salje, W. Schranz, D. E. Soto-Parra, and E. Vives, Phys. Rev. Lett. **110**, 088702 (2013).
[13]E. K. H. Salje, G. I. Lampronti, D. E. Soto-Parra, J. Baró, A. Planes, and E. Vives, Am. Minerol. **98**, 609–615 (2013).
[14]G. F. Nataf, P. O. Castillo-Villa, P. Sellapan, W. M. Krives, E. Vives, A. Planes, and E. K. H. Salje, J. Phys. Condens. Matter **26**, 275401 (2014).
[15]G. F. Nataf, P. O. Castillo-Villa, J. Baró, X. Illa, E. Vives, A. Planes, and E. K. H. Salje, Phys. Rev. E **90**, 022405 (2014).
[16]D. E. Soto-Parra, X. Zhang, S. Cao, E. Vives, E. K. H. Salje, and A. Planes, Phys. Rev. E **91**, 060401(R) (2015).
[17]T. Mäkinen, A. Miksic, M. Ovaska, and M. J. Alava, Phys. Rev. Lett. **115**, 055501 (2015).
[18]J. Baró, P. Shyu, S. Pang, I. M. Jasiuk, E. Vives, E. K. H. Salje, and A. Planes, Phys. Rev. E **93**, 053001 (2016).
[19]V. Navas-Portella, I. Serra, A. Corral, and E. Vives, Phys. Rev. E **97**, 022134 (2018).
[20]E. K. H. Salje, A. Planes, and E. Vives, Phys. Rev. E **96**, 042122 (2017).
[21]A. Clauset, C. Shalizi, and M. Newman, SIAM Rev. **51**, 661–703 (2009).